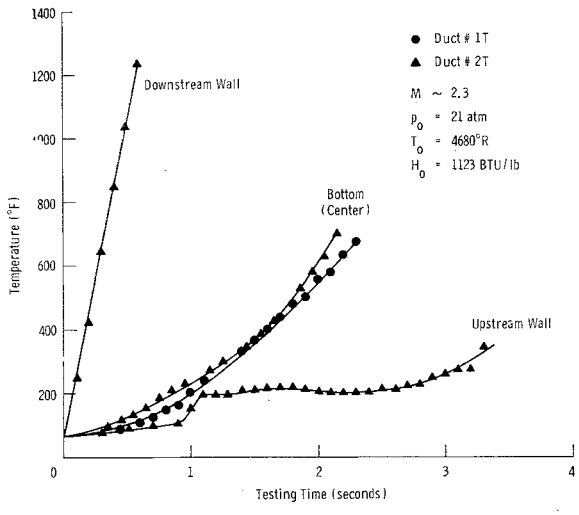

Fig. 3 Temperature variation for longitudinal cracks.

Results

For the laminar tests,[3] it was found that ablation induces transition at a Reynolds number, Re_θ, of 450. This is supported by numerical results[3] and the longitudinal, almost parallel striations shown in Fig. 2. At the downstream side of the longitudinal crack a pronounced wake-like additional ablation pattern is observed. The transverse crack shows only a slight rounding on the downstream side. The heating rates at the bottom of the longitudinal and transverse cracks are 0.24 Btu/ft² sec and a maximum of 0.07 Btu/ft² sec, respectively. In terms of q/q_s, the values are 0.0042 and 0.0016, respectively, where q_s has been computed by the transient version of the numerical code.[3]

Ablation was very pronounced during the turbulent tests. It was relatively uniform, varying from 0.159 lb/ft² sec near the duct entrance to 0.115 lb/ft² sec along the duct. This corresponds to $\dot{m}/\rho_\infty u_\infty St \simeq 0.99$. Criss-cross striation patterns (Fig. 2) were exhibited by all ducts of the turbulent test series. The patterns start close to the duct entrance and form in a uniform fashion if a pressure orifice is not located there. The cracks have a pronounced effect on the striation patterns; they alter the spacing or even cause them to disappear. At the downstream side of longitudinal cracks a complex pattern and severe gouging is observed.

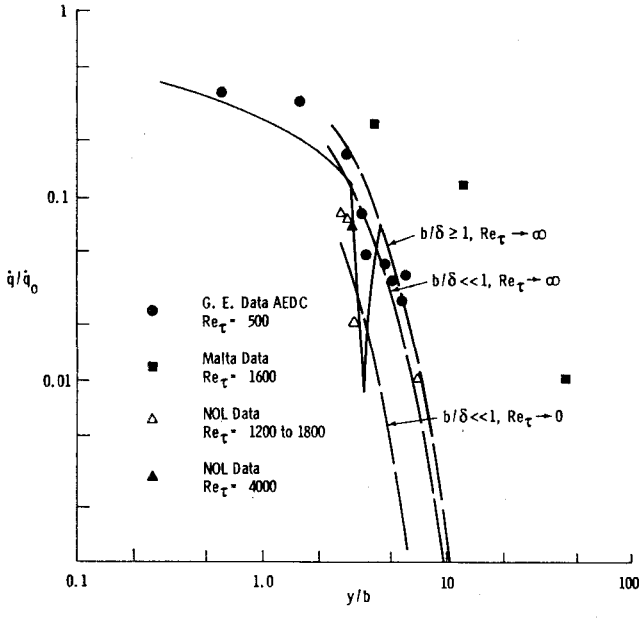

Fig. 4 Transverse crack heating summary (curves and Non-NOL data courtesy of the aeronautical research associates of Princeton).

At the longitudinal cracks, 1 in. × $\frac{1}{32}$ in., the center of the downstream wall experiences the cold-wall surface heating rate. At the bottom of the cracks the heating rate varies first slowly but it reaches the surface heating rate within two seconds (Fig. 3). A faint pattern of transverse vortices is discernible at the bottom of the cracks. The center of the upstream wall showed an erratic behavior probably indicative of a changing vortex formation. The transverse crack heating rates are moderate.

From the limited number of tests, the following observations can be made for the tests with turbulent boundary layers: 1) For initial aspect ratios of 4, the heat transfer to the bottom of transverse cracks reaches up to 8% of the duct surface heat transfer within six seconds. There is evidence of gouging due to vortices that had established in the cracks. 2) The h/b, b/δ^*, or Re_τ do not seem to be unique correlating parameters. 3) With increasing h, the heat transfer decreases very sharply and is only 1.0–1.8% of the surface heating rate. This behavior is consistent with the analytical predictions,[4] as shown in Fig. 4. 4) In short duration runs, the temperature rises uniformly. For longer runs, a periodic behavior is exhibited. A uniform temperature rise is followed by a period where the temperature remains constant, or even decreases, then the temperature rises again at about the initial rate. This observation strongly suggests that vortex flow exists in the cracks with the number of counter-rotating vortices being some multiple of the crack width. As, with ablation, the crack height is reduced and the width increased so that the vortex at the bottom can no longer be maintained, this vortex breaks up and the gas becomes more or less stagnant. The bottom temperature remains constant until the next vortex has reached the bottom or a reformation has taken place to fit the changed geometry.

References

[1] Haugen, R. L. and Dhanak, A. M., "Heat Transfer in Turbulent Boundary-Layer Separation over a Surface Cavity," *Journal of Heat Transfer, Transactions of the American Society of Mechanical Engineers*, Vol. 89, Series C, Nov. 1967, pp. 335–340.

[2] Winkler, E. M. et al., "Investigation of Substructure Heating on Cracked Ablative Heat Shields," NOLTR 69-122, July 1969, Naval Ordnance Lab., White Oak, Md.

[3] Winkler, E. M. et al., "Supersonic Ablation Studies with Teflon," NOLTR 69-125, Oct. 1969, Naval Ordnance Lab., White Oak, Md.

[4] Donaldson, C. duP. and Dunn, J. E., "Final Report on Flow and Heat Transfer Studies in Transverse Cracks," Rept. 133 (DASA Rept. 2301), June 1969, Aeronautical Research Associates of Princeton, Inc., Princeton, N. J.

Radiative Cooling of Shock-Heated Air in Cylindrical Shock Tubes

KUEI-YUAN CHIEN* AND DALE L. COMPTON†
NASA Ames Research Center, Moffett Field, Calif.

THE purpose of this note is to extend the work of Ref. 1 by presenting parametric computations of enthalpy profiles for nonadiabatic flow of air behind a nonattenuating incident shock wave in a cylindrical shock tube. The parameters and their variations in this study are: shock velocity

Received May 6, 1970.

* National Academy of Sciences–National Research Council Postdoctoral Research Associate. Member AIAA.

† Research Scientist. Associate Fellow AIAA.

U_∞,10–20 km/sec; postshock pressure p_s, 0.3, 1, and 3 atm; shock-tube radius R, 4.7 and ∞ cm; distance L from shock wave to interface between driver and driven gas, 4.7 and 9.4 cm. The gas is nongrey, and both axial and radial radiative transfer are permitted. Sufficient results are presented here to enable the shock-tube researcher to estimate quantitative enthalpy distributions for shock tubes of other sizes operated at other conditions.

The present results show that radiative cooling can signficantly affect the flowfield for shock velocities greater than about 10 km/sec. For example, at a shock velocity of 14 km/sec and a postshock pressure of 1 atm (typical of conditions attainable in both explosively driven[2] and high-performance arc-driven[3] shock tubes), the enthalpy at 3 cm behind the shock wave is reduced to about 80% of the Rankine-Hugoniot value by radiative cooling, and the density is correspondingly increased. Changes such as these in thermodynamic properties have, of course, considerable influence on the radiation itself. In addition, they produce a nonuniform flow that would be of concern for tests employing a fixed model, or for studies using the region behind the reflected shock wave.

The basis for the present computations is given in detail in Ref. 1 and will be abstracted only briefly here. The geometrical arrangement is a cylindrical shock tube, with shock-fixed axial coordinate x and radial coordinate r. The radiating volume is a right-circular cylinder of length L and radius R. The flow is assumed to be inviscid, nonconducting, in local thermodynamic equilibrium, and steady in shock-fixed coordinates. An order-of-magnitude analysis on the equations of motion shows that it is reasonable to assume constant pressure behind the shock wave. It follows then that radial motion can be neglected and that the axial mass flux is constant. With these assumptions we need solve only the energy equation to compute the enthalpy field $h(x,r)$ behind the shock wave. That equation reduces to

$$\rho_\infty U_\infty \frac{\partial h(x,r)}{\partial x} = -\nabla \cdot \mathbf{q} = -\int_0^\infty \alpha_\nu \left(4\pi B_\nu - \int_0^{4\pi} I_\nu d\Omega\right) d\nu \tag{1}$$

where ρ_∞ is the freestream density. The quantity $\nabla\cdot\mathbf{q}$ is the divergence of the radiative heat-flux vector, and is given by the expression on the right-hand side of Eq. (1). In that expression ν is optical frequency, Ω is solid angle, and α_ν, I_ν, and B_ν are, respectively, the monochromatic absorption coefficient, radiative specific intensity, and Planck function.

The present solution of Eq. (1) is performed on the basis of the differential approximation for raditive transfer[4] for

Table 1 Normalized enthalpy distributions h/h_s for p_s = 0.3 atm, R = 4.7 cm, L = 4.7 cm

		x, cm					
r/R	U_∞, km/sec	0.5	1	2	3	4	4.7
0	10	0.998	0.996	0.992	0.989	0.986	0.983
	12	0.980	0.969	0.944	0.923	0.904	0.891
	14	0.968	0.939	0.894	0.854	0.819	0.795
	16	0.957	0.919	0.852	0.799	0.751	0.720
	18	0.954	0.911	0.835	0.769	0.708	0.669
0.5	10	0.998	0.996	0.992	0.989	0.985	0.983
	12	0.979	0.968	0.941	0.920	0.900	0.887
	14	0.967	0.938	0.891	0.849	0.813	0.789
	16	0.956	0.916	0.847	0.792	0.743	0.712
	18	0.953	0.908	0.828	0.761	0.699	0.659
1	10	0.997	0.995	0.991	0.987	0.983	0.980
	12	0.977	0.962	0.932	0.907	0.884	0.870
	14	0.963	0.930	0.874	0.827	0.787	0.761
	16	0.951	0.905	0.825	0.761	0.707	0.674
	18	0.946	0.891	0.799	0.725	0.656	0.613

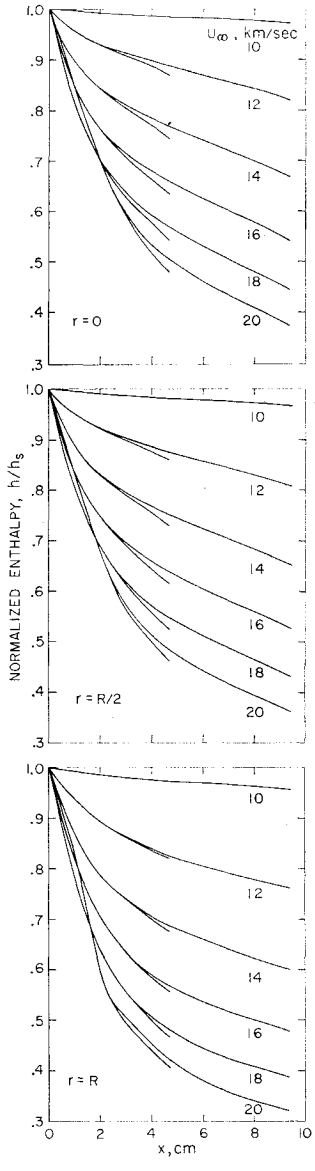

Fig. 1 Axial enthalpy profiles for p_s = 1 atm; R = 4.7 cm, L = 4.7 and 9.4 cm.

which the governing equations are

$$\nabla\cdot\mathbf{q}_\nu = \alpha_\nu(4\pi B_\nu - I_\nu^0) \tag{2a}$$

$$\nabla I_\nu^0 = -3\alpha_\nu \mathbf{q}_\nu \tag{2b}$$

where

$$I_\nu^0 \equiv \int_0^{4\pi} I_\nu d\Omega$$

Equation (2a) is exact, whereas Eq. (2b) is an approximation for the integral over solid angle of I_ν.

We assume that all radiation reaching a boundary surface (i.e., the shock wave, the interface between driver and driven gas, and the shock-tube sidewall) is lost from the gas and that there is no incoming radiation from any external source. This gives an upper limit to the radiative loss since the effects of upstream absorption, of finite wall reflectivity, and of hot driver gases will all be to reduce the enthalpy loss from the gas. These assumptions lead to the following boundary conditions for the differential approximation: $I_\nu^0(0,r) + 2q_\nu^x(0,r) = 0$ at the shock front, $I_\nu^0(L,r) - 2q_\nu^x(L,r) = 0$ at the interface, and $I_\nu^0(x,R) - 2q_\nu^r(x,R) = 0$ at the sidewall. There is also the symmetry condition $q_\nu^r(x,0) = 0$ at the tube centerline. Immediately behind the shock front the enthalpy is assumed to be given by $h_s = U_\infty^2/2$.

The model used to approximate the spectral variation of the absorption and emission properties of high-temperature

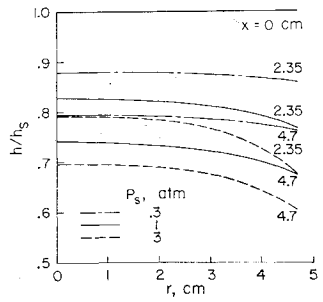

Fig. 2 Radial enthalpy profiles for U_∞ = 14 km/sec; R = 4.7 cm, L = 4.7 cm.

air is essentially that described in Ref. 5, modified slightly as described in Ref. 1. As modified, this model has four grey bands that, collectively, include contributions from both continuum and line radiation over the complete optical spectrum. With this model, the frequency integral in Eq. (1) can be expressed as a four-term sum, thus greatly simplifying the computations. At the highest velocity considered here (20 km/sec), the model is somewhat less reliable because it does not include radiative processes that involve doubly ionized nitrogen or oxygen.

Solutions to Eqs. (1) and (2) are obtained by expanding the dependent variables I_ν^0 and h in power series in r^2 with coefficients that depend on the axial variable x. In all the present solutions only the first three terms are retained in these series. The accuracy of the differential approximation with this three-term solution was investigated for the present geometry in Ref. 1 by comparison with solutions of Eq. (1) in which the integral of $I\nu$ over solid angle was not approximated [as in Eq. (2b)], but was performed numerically. These comparisons were at a shock velocity of 16 km/sec and were for the same four-band spectral model as used here. They showed that the differential approximation with the three-term solution is adequate for computation of the enthalpy loss (maximum error in enthalpy of about 8%), but is somewhat deficient in its ability to reproduce accurately the curvature of the radial enthalpy profiles near the wall. Neither the curvature deficiency nor the maximum error is expected to be more serious for any of the results presented here than for those of Ref. 1.

Normalized axial enthalpy profiles h/h_s at r = 0, $R/2$, and R are shown in Fig. 1 for p_s = 1 atm, with shock velocity as a parameter. Except for the highest velocity (20 km/sec), the profiles show a successively greater decrease in normalized enthalpy near the shock front as velocity increases. It should be noted, however, that the dimensional enthalpy h at a given x and r always increases with increasing U_∞. At the lowest velocity (10 km/sec), the enthalpy decrease is small, less than 5%, while at the highest velocity the enthalpy decreases to less than one-half its initial value. The curves for U_∞ = 20 km/sec are probably less accurate than those for the lower velocities because of the neglect of the radiative processes due to the presence of N^{++} and O^{++}

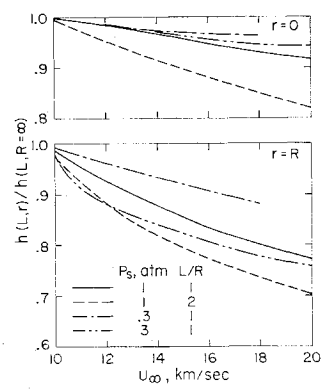

Fig. 3 Comparison of solutions for R = 4.7 cm with corresponding solutions for R = ∞.

Table 2 Normalized enthalpy distributions h/h_s for p_s = 3 atm, R = 4.7 cm, L = 4.7 cm

		x, cm					
r/R	U_∞, km/sec	0.5	1	2	3	4	4.7
0	10	0.996	0.993	0.988	0.984	0.980	0.977
	12	0.960	0.938	0.910	0.885	0.863	0.840
	14	0.906	0.861	0.808	0.767	0.730	0.696
	16	0.860	0.791	0.718	0.665	0.621	0.582
	18	0.826	0.733	0.643	0.585	0.534	0.490
	20	0.826	0.689	0.581	0.519	0.465	0.420
0.5	10	0.996	0.993	0.987	0.982	0.978	0.975
	12	0.957	0.934	0.901	0.876	0.853	0.829
	14	0.901	0.851	0.794	0.752	0.716	0.684
	16	0.852	0.779	0.702	0.648	0.604	0.566
	18	0.820	0.717	0.623	0.565	0.515	0.475
	20	0.820	0.677	0.559	0.495	0.445	0.403
1	10	0.994	0.988	0.979	0.970	0.964	0.960
	12	0.927	0.880	0.825	0.790	0.769	0.755
	14	0.847	0.767	0.691	0.652	0.623	0.603
	16	0.794	0.673	0.581	0.541	0.512	0.490
	18	0.778	0.617	0.490	0.453	0.426	0.403
	20	0.801	0.610	0.431	0.386	0.358	0.336

as mentioned earlier. Results for two values of L are also given in Fig. 1. Comparison of these results shows that the effect of the change in L is confined to a region near x = L, and that, even in that region, the effect is not large.

Enthalpy distributions for p_s = 0.3 and 3 atm are tabulated as a function of shock velocity in Tables 1, and 2, respectively. Figure 2 shows normalized radial enthalpy profiles for a representative velocity (14 km/sec), and for all three pressures. This figure illustrates that, as pressure increases, there is both more enthalpy decrease (because of higher emission) and more curvature near the wall in the radial profiles (because of greater optical thickness).

Figure 3 shows the ratio of the enthalpy at the interface for R = 4.7 cm to that for R = ∞. (In effect, setting R = ∞ corresponds to using a one-dimensional radiative transfer analysis.) This ratio is shown for both the centerline and sidewall of the tube. Near the centerline the one-dimensional calculations are not too seriously in error (less than 10%) for L/R = 1 (corresponding to a cylinder with a diameter twice its length), but when L/R = 2, the one-dimensional calculations are inadequate. For r = R, the one-dimensional calculations are always inadequate, as is to be expected.

In conclusion, we note that the computational technique used here is efficient, computation times were typically 5–10 min/case on the IBM 7094. With this technique, computations could also be performed for other gases, assuming of course the availability of a spectral model.

References

[1] Chien, K.-Y. and Compton, D. L., "Flow in a Cylindrical Shock Tube With Radiative Energy Loss," *Proceedings of the 1970 Heat Transfer and Fluid Mechanics Institute*, Monterey, Calif. June 10–12, 1970, pp. 278–293.

[2] Berggren, R. E. et al., "'Ames' High-Explosive Shock-Tube Facility," *Proceedings of the Seventh International Shock Tube Symposium*, Toronto, Canada, June 23–25, 1969.

[3] Dannenberg, R. E., "An Imploding Trigger Technique for Improved Operation of Electric Arc Drivers," *Proceedings of the Seventh International Shock Tube Symposium*, Toronto, Canada, June 23–25, 1969.

[4] Vincenti, W. G. and Kruger, C. H., Jr., *Introduction to Physical Gas Dynamics*, Wiley, New York, 1965, Chap. XII.

[5] Page, W. A. et al., "Radiative Transport in Inviscid, Nonadiabatic Stagnation-Region Shock Layers," *AIAA Selected Reprints*, Vol. VII, *Radiative Gas Dynamics*, edited by R. J. Goulard, 1969, pp. 51–65.